AGU100 ADVANCING EARTH AND SPACE SCIENCE

JGR Biogeosciences

RESEARCH ARTICLE
10.1029/2018JG004833

Key Points:
- A field investigation of the impact of Kuroshio Current on the microbial metabolism in the oligotrophic northern South China Sea basin
- Increases heterotrophic bacterial activity and primary production were associated with the Kuroshio Current intrusion
- A shift of metabolic status from the net heterotrophy to the prevailing autotrophy was observed in the mixing zone

Supporting Information:
- Supporting Information S1

Correspondence to:
B. Huang,
bqhuang@xmu.edu.cn

Citation:
Huang, Y., Laws, E., Chen, B., & Huang, B. (2019). Stimulation of heterotrophic and autotrophic metabolism in the mixing zone of the Kuroshio Current and northern South China Sea: Implications for export production. *Journal of Geophysical Research: Biogeosciences*, *124*, 2645–2661. https://doi.org/10.1029/2018JG004833

Received 26 SEP 2018
Accepted 17 JUL 2019
Accepted article online 16 AUG 2019
Published online 3 SEP 2019

Stimulation of Heterotrophic and Autotrophic Metabolism in the Mixing Zone of the Kuroshio Current and Northern South China Sea: Implications for Export Production

Yibin Huang[1,2], **Edward Laws**[3], **Bingzhang Chen**[4], **and Bangqin Huang**[1,2]

[1]State Key Laboratory of Marine Environmental Science, Xiamen University, Xiamen, China, [2]Fujian Provincial Key Laboratory of Coastal Ecology and Environmental Studies, Xiamen University, Xiamen, China, [3]Department of Environmental Sciences, College of the Coast and Environment, Louisiana State University, Baton Rouge, LA, USA, [4]Department of Mathematics and Statistics, University of Strathclyde, Glasgow, UK

Abstract To evaluate the influences of the Kuroshio Current intrusion on the biogeochemistry of the northern South China Sea (NSCS), we conducted field observations of the responses of microbial metabolism to the intrusions of the Kuroshio Current into the NSCS. We used an isopycnal mixing model to quantitatively assess the extent of the Kuroshio intrusion into the NSCS and found that bacterial abundance, production, and growth efficiency were unimodal functions of the fraction of Kuroshio water. Values were maximal at ~60% Kuroshio water and decreased monotonically as the percent of Kuroshio water deviated from 60%. The patterns of gross primary production and nitrate concentration were similar, but the peaks occurred at ~50% Kuroshio water. The Kuroshio intrusion, however, had little impact on bacterial and community respiration. The observed elevation of nitrate concentrations at ~50% Kuroshio water was quantitatively consistent with estimates of the amount of inorganic nitrogen released by remineralization of dissolved organic nitrogen by bacteria. Based on these observations, we hypothesize that dissolved organic matter in the Kuroshio water stimulates bacterial activity, and catabolism of the dissolved organic matter releases inorganic nutrients that stimulate primary production in the NSCS basin. The concomitant elevation of net community production subsequently enhances export production and thereby strengthens the biological pump in the nitrogen-limited NSCS basin. Recognition of this mechanism underscores the role of horizontal currents in regional carbon and nitrogen cycles and broadens understanding of the processes that sustain export production in the oligotrophic ocean.

Plain Langue Summary Horizontal currents universally occur in the global ocean; however, the knowledge of associated impacts in the biogeochemical processes is still poorly represented. We first estimate the degree of horizontal Kuroshio Current in the different sampling stations in the oligotrophic regime of northern South China Basin. Then we found the significant increase of autotrophic primary production, heterotrophic bacterial abundance, and bacterial production in the regions with a moderate fraction of Kuroshio water. Such changes led to higher net community production. We further linked the observations of changes in nutrient pools with the microbial activities to figure out a more comprehensive picture of the impact of the Kuroshio Current in biogeochemical processes in the northern South China Basin. As the ocean is toward greater processes relative to the vertical processes due to more stratification in the upper water, our study is also a step forward understanding the potential feedbacks of marine to the climate change.

1. Introduction

Nearly half of the primary production on Earth occurs in the ocean (Falkowski et al., 2003), and plankton-mediated carbon transfer from the atmosphere into the ocean interior, namely, the *soft-tissue biological pump*, plays a critical role in regulating atmospheric CO_2 levels on geological timescales (Siegel et al., 2014; Sigman & Boyle, 2000). Photosynthesis captures CO_2 from the atmosphere and provides most of the organic carbon for aquatic heterotrophs, whereas heterotrophic activity subsequently releases the carbon back into the atmosphere as CO_2. Among the various heterotrophs, bacteria consume a large amount of

the organic carbon (del Giorgio et al., 1997) and play a fundamental role in recycling through the microbial loop (Azam et al., 1983; Ducklow, 1999). The magnitude of microbial metabolism in the upper water column is therefore an important determinant of the efficiency of oceanic CO_2 uptake and ocean-atmosphere coupling within the climate system.

In the oligotrophic ocean, the largest biome on Earth, current understanding of the mechanism that controls microbial activity has focused mainly on proximate factors (i.e., light, nutrients, and community structure) and associated temporal variability (Gist et al., 2009; Jenkins & Doney, 2003; Viviani & Church, 2017). However, recent observations have indicated that proximate factors are insufficient to explain the observed biogeochemical variability with depth, even in the central gyres (Johnson et al., 2010; Lozier et al., 2011). This inadequacy has led to more attention being paid to the potential influence of horizontal currents. Previous studies have been focused mainly on elucidating hydrographic changes and physical dynamics (Hu et al., 2015; Huthnance et al., 2009). The impacts of currents on biogeochemical processes have received relatively little attention (Abell et al., 2000; Fontes et al., 2018; Reynolds et al., 2014). Based on a global circulation model, Letscher et al. (2016) have demonstrated that organic matter transported by currents could account for a considerable fraction of export production in the oligotrophic ocean and as much as 24–36% of nitrogen export and 40–67% of phosphorus export on a global scale. The inorganic nutrients transported by horizontal currents have been observed to be rapidly consumed near-gyre margins, but the transport of organic matter is commonly assumed to precede remineralization of the organic matter into inorganic compounds (Bronk et al., 2007; Letscher et al., 2016). The mechanism of how currents contribute to the biogeochemical cycling of carbon remains unclear because of the paucity of field investigations of biogeochemical responses to horizontal advection and mixing.

The South China Sea is the world's largest marginal sea in the western Pacific Ocean. The northern South China Sea (NSCS) basin during the warm season is typically a nitrogen-limited ecosystem. It is characterized by low nitrate concentrations, primary production, and export production (Liu et al., 2002; Ning et al., 2004) because of strong stratification in the upper water column (Wong et al., 2007) and relatively little nitrogen fixation (Lee Chen et al., 2008). However, the NSCS basin is characterized by dynamic interactions with the adjacent Pacific Ocean through the Luzon Strait (Dai et al., 2013; Nan et al., 2015). The Kuroshio Current, the western boundary current of the North Pacific subtropical gyre, flows from roughly 15° to 35° north latitude (Hu et al., 2015). Over the course of 1 year, the Kuroshio Current frequently intrudes into the NSCS via the Luzon Strait. The vertical distribution of the currents through the strait mimics a sandwich structure: Water enters the NSCS at depths of 0–400 m and ~1,500–3,000 m, and it returns to the western Pacific Ocean at intermediate depths of ~500–1,500 m (Dai et al., 2013; Nan et al., 2015; Qu et al., 2000). The Kuroshio Current is typically characterized by warmer and more saline water but extremely low nutrient concentrations relative to the NSCS (Du et al., 2013). The relatively deep nitracline of the Kuroshio favors the growth of *Trichodesmium* and high N_2 fixation rates (Lee Chen et al., 2008; Shiozaki et al., 2015). The Kuroshio, although oligotrophic, has been reported to have higher dissolved organic carbon (DOC) concentrations (60–79 mmol/m^3) than the NSCS (51–70 mmol/m^3) based on seasonal observations in this region (Wu et al., 2015). The unique characteristics of the Kuroshio Current and its frequent interactions with the NSCS basin thus provide an ideal laboratory for studying the effects of currents on biogeochemical processes in the oligotrophic ocean. Here, using data collected from a research cruise in the NSCS basin during a period when a significant Kuroshio intrusion was detected (Xu et al., 2018), we used an isopycnal mixing model (Du et al., 2013) to quantify the proportion of water contributed by the Kuroshio in the upper water column. Next, we analyzed concurrent measurements of autotrophic and heterotrophic metabolism together with previously published observations of nutrient pools during the same cruise to construct a more comprehensive picture of the impact of the Kuroshio Current on biogeochemical processes in the NSCS basin.

2. Methods

2.1. Study Sites

Our study area was located in the NSCS basin (Figure 1), which is effectively isolated from terrestrial inputs because of the seasonal changes of the basin-wide circulation gyre (Hu et al., 2000). During the summer, the NSCS basin is typically characterized by oligotrophic conditions, with low biomass and nutrient

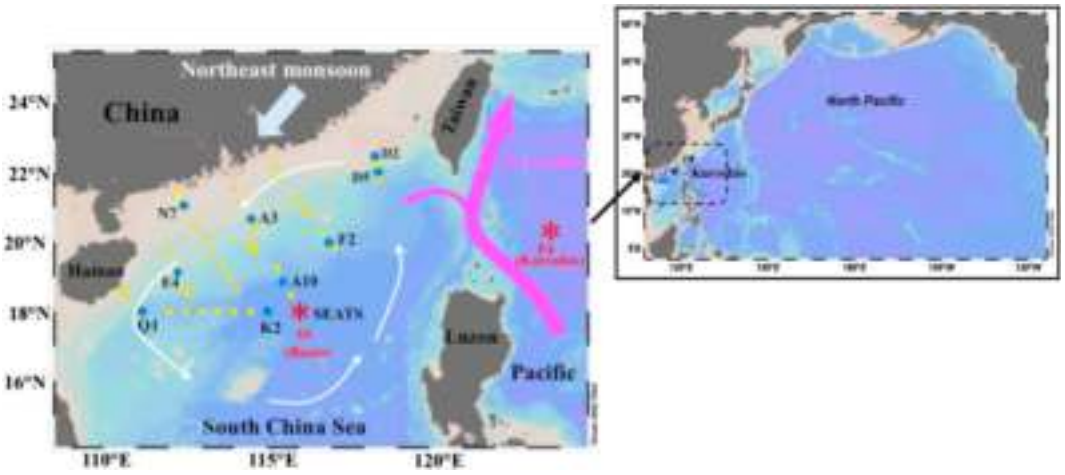

Figure 1. Map of the study area in the northern South China Sea (NSCS) from 15 May to 7 June 2016. The yellow and blue dots indicate sampling stations, at 10 of which (blue dots) incubation experiments were conducted. The white arrow represents the surface circulation in the NSCS during the northeast monsoon. The red and black stars indicate typical Kuroshio water (P4) and South China Sea water (SS), which were selected as the two end-members for the isopycnal mixing model in accord with Du et al. (2013).

concentrations due to the extensive stratification that occurs in the upper water column (Gong et al., 2003; Lee Chen & Chen, 2006). Recent studies have demonstrated that the intrusion of the Kuroshio Current into the NSCS significantly impacts the nutrient inventory, DOC pool, and nitrogen cycling in the upper 100 m of the water column (Du et al., 2013; Wu et al., 2015; Xu et al., 2018).

2.2. Chemical and Biological Assays

The research cruise was conducted from 15 May to 7 June 2016 on board the R/V *Dongfanghong II*. Forty-eight stations were visited, including 10 stations for incubation experiments (Figure 1). Samples were collected with a 24-bottle Niskin rosette system with 12-L PVC bottles. Water temperature and salinity were measured with a conductivity-temperature-depth probe (SBE 911, Sea-Bird Electronics) attached to the rosette. For each sampling depth, ~50-ml water samples were collected for determination of nutrient concentrations and preserved at −20 °C until analysis. The concentrations of nitrate plus nitrite were measured with an AutoAnalyzer (Technicon AA3, Bran-Lube, GmbH) following the procedures described in Han et al. (2012). For low-level NO_2^- and NO_3^- analyses, we used the flow injection analysis-liquid waveguide capillary cell method, which has a detection limit of 2 nmol/L (Patey et al., 2008). Ammonium concentrations were determined by the fluorometric o-phthaldialdehyde method with a detection limit of 0.7 nmol/L (Zhu et al., 2013). The chemical data from the same cruise have been published by Xu et al. (2018).

For the phytoplankton community structure, 4–5 L of seawater from each depth were filtered onto 25-mm-diameter GF/F filters under a low vacuum pressure (<40-mm Hg). The filters were stored in liquid nitrogen before the pigments were extracted with 2 ml of N,N-dimethylformamide for 2 hr in the dark at 2–8 °C. Phytoplankton pigment concentrations were measured by high-performance liquid chromatography. The detailed analytical procedures for the high-performance liquid chromatography analysis and pigment identification have been described by Liu et al. (2016). The CHEMTAX program (Mackey et al., 1996) was used to estimate the relative contributions of taxa to the total chlorophyll *a* (Chl-*a*) based on the pigment data. Thirteen diagnostic pigments were used to associate the fractions of the total Chl-*a* pool with nine phytoplankton groups: dinoflagellates (Dino), diatoms (Diat), haptophytes (Type 8; Hapt_8), haptophytes (Type 6; Hapt_6), chlorophytes (Chlo), cryptophytes (Cryp), *Prochlorococcus* (Proc), *Synechococcus* (Syne), and prasinophytes (Pras). The initial input ratios of the diagnostic pigments to Chl-*a* (Table S2 in the supporting information) were based on ratios used in previous studies in the NSCS (Wang et al., 2016; Xiao et al., 2018).

For determination of bacterial abundance, 1.8-ml water samples were fixed with 1% (final concentration) seawater-buffered paraformaldehyde and stored at −80 °C. The bacterial abundances were enumerated

using an Accuri C6 flow cytometer (Becton, Dickinson, USA) after staining with 0.01% (final concentration) SYBR Green (Molecular Probes; Marie et al., 1997). Yellow-green latex beads (0.5 μm, Polysciences) were also added to the samples during the measurements as an internal standard.

2.3. The isopycnal Mixing Model

To quantify the impact of the Kuroshio intrusion on the NSCS basin, we adopted a well-validated, two-end-member isopycnal mixing model. The assumption behind the model was that mixing between the different water masses was dominated by isopycnal mixing, and diapycnal mixing was comparatively insignificant (Du et al., 2013). The detailed methodology and validation of this model were introduced by Du et al. (2013) and have been applied in recent studies (Wu et al., 2015; Xu et al., 2018). Briefly, we chose two representative stations, P4 (123°E, 20°N) and SS (116°E, 18°N), to represent the Kuroshio and NSCS water endpoints, respectively, for the isopycnal mixing model (Figure 1). Based on the characteristics of the end-members, the conservative equations in term of potential temperature (θ) or salinity (S) along the isopycnal plane can be expressed by equations (1) and (2):

$$R_{K\,\theta} + R_{S\,\theta} = 1 \text{ or } R_{KS} + R_{SS} = 1 \tag{1}$$

$$R_{K\,\theta} \times \theta_K + R_{S\,\theta} \times \theta_S = \theta \text{ or } R_{KS} \times S_K + R_{SS} \times S_S = S \tag{2}$$

where R_K and R_S are the fractions of Kuroshio water and NSCS water, respectively ($R_{K\theta}$ and R_{KS} represent the results derived from θ and S, respectively). The values of θ_K and S_K indicate the end-member values of θ and S for the Kuroshio water, and θ_S and S_S represent the corresponding values for the NSCS. The contribution from the Kuroshio (R_K) end-member water can then be obtained as follows:

$$R_K = R_{K\,\theta} = (\theta - \theta_S)/(\theta_K - \theta_S) \text{ or } R_K = R_{KS} = (S - Ss)/(S_K - S_s) \tag{3}$$

In the present study, salinity (S) was selected as an indicator to estimate R_k at each sampling station in accord with the study of Du et al. (2013) because θ is likely affected by heat flux (Qiu et al., 2015). Although the upper intrusion of the Kuroshio into the NSCS may extend to a depth of 400 m (Fang et al., 2009; Tian et al., 2009), the R_K values reported here are the average fractions of Kuroshio water in the upper 100 m because most of the intense biological activity occurs in the euphotic zone, which usually extends to depths of 80–100 m in our study region (Lee Chen, 2005; Tseng et al., 2005).

2.4. In Vitro Oxygen-Based Microbial Metabolism

The first conductivity, temperature, and depth probes (CTD) cast before dawn was used to collect the water sample for the incubation experiment. Microbial metabolism was derived from the changes in dissolved oxygen concentrations during 24-hr incubations (Huang et al., 2019). The dissolved oxygen concentration was determined by high-precision Winkler titration (Oudot et al., 1988) with an automated potentiometric endpoint detection system (Metrohm-848, Switzerland). This method achieves a precision of about 0.04% (coefficient of variation) at oxygen concentrations between 70 and 250 mmol O_2 m^{-3} (Furuya & Harada, 1995). Samples from five discrete depths, corresponding to 100%, 50%, the deep chlorophyll maximum (DCM), 10%, and 1% of surface irradiance (I_0) were collected at the incubation stations, where the depths of the water column exceeded 200 m. If the depth of the DCM was coincident with the base of the euphotic zone, additional depths between the depth corresponding to 10% light and the DCM were collected. The water samples were siphoned into 12 calibrated 100-ml borosilicate bottles, and ~300 ml was allowed to overflow. The dissolved oxygen in the four bottles was immediately fixed at the start of the incubation (initial bottles). Two sets of four light and four dark incubation bottles were placed in a large tank filled with water exposed to natural sunlight. The light bottles were covered with neutral density meshes to adjust the light conditions to match the in situ irradiances at the corresponding sampling depths. The incubation temperature was maintained by running surface seawater. Gross primary production (GPP) was calculated as the difference between the average dissolved oxygen concentrations in the light and dark bottles after 24-hr incubations; community respiration (CR) was equated to the difference between the average dissolved oxygen concentrations in the initial and dark bottles. The average propagated standard errors were 0.26 mmol O_2 m^{-3}/day for GPP and 0.19 mmol O_2 m^{-3}/day for CR (n = 50). Net community production (NCP) was defined as the difference between GPP and CR, and its magnitude was relatively small

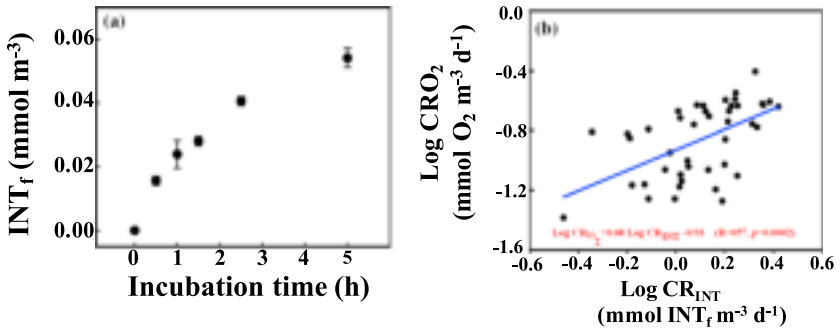

Figure 2. (a) The relationship between rates of INT_f (formazan) reductions and incubation time from a depth of 5 m at SEATS station (b) pair measurements of log-transformed community respiration (CR) derived from rates of 2–4-hr in vitro INT reductions and 24-hr rates of oxygen consumption. The blue line represents the linear relationship derived from the paired measurements of log-transformed CR.

compared to GPP and CR. Small errors in GPP (or CR) could therefore result in large errors in NCP. Given the fact that there was no pattern in the response of CR to the Kuroshio intrusion (see section 2.1), NCP at each station was estimated by subtracting the average CR at all stations from the corresponding GPP at each station.

2.5. Size-Fractionated Respiration Derived from In Vitro INT Reduction Capacity Assay

Size-fractionated respiration was estimated based on in vitro INT reduction rates as described by Martínez-García et al. (2009). The sampling depths were the same as the depths sampled for the in vitro oxygen-based microbial metabolism measurements. Four 200-ml polypropylene plastic bottles were filled with seawater. One bottle was immediately fixed by adding formaldehyde (2% w/v final concentration) as a blank. Fifteen minutes later, the four replicates were inoculated in the dark by the addition of 2-(*ρ*-iodophenyl)-3-(*ρ*-nitrophenyl)-5phenyl tetrazolium chloride salt (INT, Sigma, USA) at a final concentration of 0.8 mM. The INT samples were incubated at the same temperature as the dissolved oxygen bottles. After incubations of 2–3 hr, the reactions were stopped by adding formaldehyde. All the samples were sequentially filtered after 15 min through 0.8 and 0.2-μm pore size polycarbonate filters and stored frozen until further processing. The INT_f reduction rates were measured using a SP-8001 UV/Vis Spectrophotometer at 485 nm following the procedure of Martínez-García et al. (2009).

A time-course experiment was conducted during the same research cruise at the surface at the SEATS station. The optimal incubation time was found to be <4 hr (Figure 2a). Therefore, all our incubations were undertaken for <4 hr. INT reduction rates were converted to oxygen units using the linear relationship: Log CR_{O2} = 0.68 Log CR_{INT} − 0.93 (r = 0.57, p = 0.002) derived from comparisons of paired measurements of CR_{INT} and CR_{O2} (Figure 2b). Bacterial respiration (BR) was defined as the respiration contributed by the 0.2–0.8-μm size fraction (García-Martín et al., 2017).

2.6. Bacterial Production

Bacterial production (BP) was estimated using the ^{3}H-leucine incorporation methods Kirchman (2001) Four 1.8-ml aliquots of water from each depth were incubated with a saturating concentration (10 nmol/L) of ^{3}H-leucine (Perkin Elmer, USA) for 2 hr in the dark. One sample was immediately killed by adding 100% trichloroacetic acid (TCA) as a control, and the other three reactions were terminated with TCA at the end of the incubation. The samples were filtered onto 0.2-μm polycarbonate filters (GE Water & Process Technologies). The filters were washed twice with 3-ml 5% TCA and twice with 2-ml 80% ethanol before being frozen

at −20 °C. Upon return to the lab, radioactivity retained on the samples was measured as disintegrations per minute using a Tri-Carb 2800TR liquid scintillation counter (Perkin Elmer, USA). To convert the incorporation of leucine to carbon units, we used a factor of 1.5 kg C mol leucine^{-1}, assuming no isotopic dilution. Bacterial growth efficiency (BGE) was equated to BP/(BR + BP). BR was converted to a carbon basis using a respiratory quotient of 0.9 for calculation of BGE (Hedges et al., 2002; Laws, 1991).

2.7. Estimates of the Amount of Inorganic Nitrogen Released by Bacterial Catabolism at ~60% Kuroshio Water

Bacteria utilize organic matter in two ways: Some of the organic matter is incorporated into bacterial biomass; the remainder is catabolized and released back into the seawater in inorganic form. The total bacterial demand for organic matter is the sum of the amount of organic matter assimilated into bacterial biomass and respired. Our measured BGE, which was derived from the ratio of carbon-based BP to the total bacterial carbon demand, was a metric of the efficiency of organic carbon utilization by the bacteria. The total bacterial nitrogen demand can likewise be expressed as the sum of the bacterial biomass nitrogen (BB_N) requirement and the amount of nitrogen remineralized via bacterial catabolism (BC_N). Based on the in situ observations of bacterial abundance and BGE in terms of carbon utilization, we could roughly estimate the amount of BC_N by the empirical nitrogen content of bacterial biomass and assuming the bacterial nitrogen regeneration efficiency is similar with the carbon regeneration efficiency. If we hypothesize that our observed elevation of inorganic nitrogen concentration (NH_4^++NO_3^-) in 60% Kuroshio water was due mainly to bacterial decomposition of DON from the Kuroshio (see section 2.2), we would expect that the BC_N would be quantitatively consistent with the observed increase of the inorganic nitrogen concentration in the seawater. There is no a priori reason, however, that the BGEs are the same for carbon and nitrogen, particularly if the C:N ratios of the substrate and bacterial biomass differ. Goldman et al. (1987), for example, have reported that the BGE is higher (lower) for carbon than for nitrogen if the C:N ratio of the substrate is lower (higher) than the C:N ratio of the bacterial biomass. Because we had no information on the C:N ratio of the dissolved organic matter used by the bacteria, we assumed the BGEs to be the same for carbon and nitrogen.

To account for the effect of mixing on the two water masses, we first calculated what the concentrations of bacteria and inorganic nitrogen would be in the absence of any sources or sinks (Table 2). For example, the theoretical bacterial abundance at $R_K = 60\%$ was estimated to be 40% of the bacterial abundance at $R_K = 0$ plus 60% of the bacterial abundance at $R_K = 100\%$. The values corresponding to $R_K = 0$ and $R_K = 60\%$ were derived from the intercepts of the linear regressions in Figures 3 and 4 to $R_K = 0\%$ and $R_K = 100\%$. The anomaly of bacterial nitrogen biomass (ΔBB_N) was equated to the anomaly of bacterial abundance multiplied by the product of the empirical bacterial carbon content (20 fg C $cell^{-1}$; Fukuda et al., 1998) and the N:C elemental ratio (1:5) for marine bacteria reported by Goldman et al. (1987). Then BC_N was equated to the difference between ΔBB_N/BGE and ΔBB_N. The BGE here was assumed to be 20–24% based on our in situ measurement near $R_K = 60\%$ (see section 2.1 and Figure 8f). We compared the calculated BC_N to the anomaly of the in situ NH_4^++NO_3^- concentration in the seawater, which was equated to the difference between the measured NH_4^++NO_3^- concentration and the theoretical value calculated from mixing of the two endpoint concentrations at $R_K = 0$ and $R_K = 60\%$.

2.8. Statistical Analysis

Areal rates within the euphotic zone were calculated by trapezoidal integration of the volumetric data from the surface down to the depth of 1% incident irradiance. The standard errors for integrated values were estimated by propagating the errors of the independent measurements in accord with Miller and Miller (1988). The data (except for NCP because some NCPs were negative) were log-transformed to satisfy the assumption of normality, which was examined (after transformation) via a Kolmogrov-Smirnov test. Many of the measured variables (i.e., nitrate, BA, GPP, and BGE) were unimodal functions of R_K and passed through a maximum at intermediate R_K values (see section 2.1). The implication is that there was a *source* between the two endpoints at $R_K = 0\%$ and $R_K = 100\%$. In other words, if there were no source or sink of these variables, all the data would lie on a straight line between the end points. Equation (3) assumes this to be the case for salinity. We therefore hypothesized that there existed an optimum fraction ($R_{K\mathrm{opt}}$) of Kuroshio water that corresponded to the maxima of these variables and that these maxima reflected admixture of Kuroshio water containing an essential factor lacking in NSCS water with NSCS water containing another essential factor lacking in Kuroshio water. To test this hypothesis, the variables were first divided into two groups of R_K values higher than and lower than an assumed intermediate value of R_K, and the two sets of variables were fit separately to straight lines with a common intercept, which we equated to $R_{K\mathrm{opt}}$. The first line was used to describe the tendency of the metrics with R_K less than $R_{K\mathrm{opt}}$, and the second line was used to describe the data with R_K greater than $R_{K\mathrm{opt}}$. The statistical significance of this piecewise linear function was

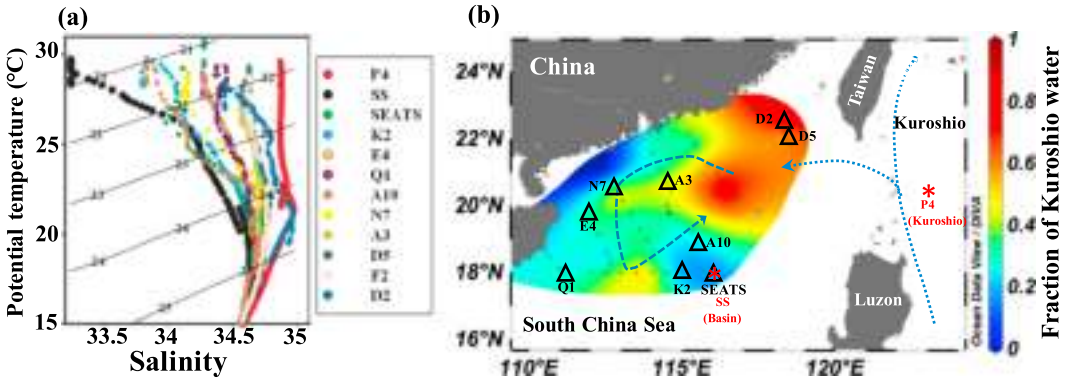

Figure 3. (a) Potential temperature versus salinity at the incubation stations. The black numbers indicate the potential density anomaly (kg/m^3). The red and black data indicate typical Kuroshio water (P4) and South China Sea water (SS), which were selected as the two end-members for the isopycnal mixing model according to Du et al. (2013). (b) The average fractions of Kuroshio water (upper 100 m) in the NSCS during the cruise. The triangles indicate the station with incubation experiment.

determined by comparing the difference between the sum of the squared deviations of the piecewise linear function from the data to the right and left of R_{Kopt} and the sum of the squared deviations of a horizontal line through the mean of all data with the sum of the squared deviations from the regression lines using an F test with 2 and $N - 3$ degrees of freedom, where N is the total number of data points and 3 is the number of adjustable parameters (one intercept and two slopes) in the piecewise linear model. The Type I error rate (p value) associated with this F statistic was determined using R software (Core, 2014). The division of two subsets was conducted under the condition that piecewise linear function gave the best fit to the data (lowest Type I error rate; i.e., the sum of the squared deviations of the data from the piecewise linear function was as small as possible, Table 1). The relationship was judged to be significant if the Type I error rate (p) was less than 0.05. Figures 1 and 3 were plotted by software Ocean Data View (Schlitzer, 2012). The complete data set is available in the supporting information and has also been deposited in the public global respiration database: https://www.uea.ac.uk/environmental-sciences/people/profile/carol-robinson#researchTab (data set is maintained by Carol Robinson).

3. Results

3.1. Kuroshio Intrusion and N-Based Nutrients

A full description of the Kuroshio intrusion and nutrient concentrations during the sampling period has been reported in Xu et al. (2018). As seen from the T-S diagram (θ-S) in Figure 3a, the hydrologic characterization of incubation stations indicated a mixture of NSCS and Kuroshio water, and all the data points fell within limits defined by the two representative end-members: SCS water (SS) and Kuroshio water (P4). At potential density anomalies (σ_θ) < 25.8 kg/m^3, the Kuroshio water tended to show higher potential temperature and salinity than the NSCS water on the same isopycnal (Figure 3a). The contour plot showed a clear

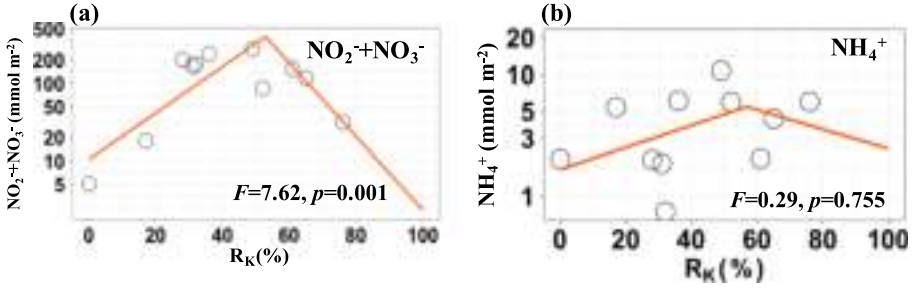

Figure 4. (a) Integrated NO_3^- concentration and (b) integrated NH_4^+ versus the fraction of Kuroshio intrusion in the upper 100 m (R_K). The NH_4^+ and NO_3^- data were compiled from Xu et al. (2018). The data on the ordinate are plotted on a logarithmic scale. The F and p represent the F statistic and its associated Type I error rate, respectively.

Table 1
Statistical Analysis of Goodness of Fit of Piecewise Linear Model to Euphotic Zone-Integrated Variables Versus the Fraction of Kuroshio water (R_K)

Variable	R_{opt} (%)	F ratio	Significance (p)
NH_4^+	56	0.29	0.755
NO_3^-	**52**	**7.62**	**0.001**
Chlorophyll *a*	-	-	-
Bacterial abundance	**67**	**8.69**	**0.001**
Gross primary production	**53**	**16**	**0.02**
Community respiration (O_2)	61	2.7	0.078
Net community production	**53**	**10.3**	**0.008**
Bacterial production	**59**	**6.54**	**0.003**
Bacterial respiration	51	1.3	0.320
Bacterial growth efficiency	**66**	**3.9**	**0.042**

Note. The F statistic was used to judge whether the piecewise linear model was a significant improvement over a horizontal line in describing the data. Significant effects are in bold ($p < 0.05$). R_{opt} is the value of R_K corresponding to the maximum of the piecewise linear function.

pathway of Kuroshio intrusion into the NSCS basin via the Luzon Strait, with a higher fraction of Kuroshio water near the eastern and northern parts of the basin (Figure 3b). At our incubation stations, the estimated R_K in the upper 100 m obtained from the two-member model varied between 0.17 at station SEATS and 0.79 at station D2 (Figure 3b).

The integrated NO_3^- concentration within the upper 100 m ranged between 5 and 276 mmol/m^2 (Figure 4a). The integrated NO_3^- concentration reached a maximum at an R_K of ~50% (Figure 4a). The statistical analysis indicated that the piecewise linear model was a significant improvement over a horizontal line in describing the data ($F = 7.62$, $p = 0.001$, Table 1 and Figure 4a). The integrated NH_4^+ concentrations were 1 order magnitude lower than the integrated NO_3^- concentrations and varied between 0.77 and 10.7 mmol/m^2 (Figure 4b). The peak value of the integrated NH_4^+ concentrations was coincident with the maximum of the integrated NO_3^- concentrations at an R_K of 50%, but the piecewise linear model was not a significant improvement over a horizontal line in describing the data ($F = 0.29$, $p = 0.755$, Table 1 and Figure 4b).

3.2. Phytoplankton Community Structure and Bacterial Abundance

The integrated Chl-*a* concentrations at our sampling stations were relatively low and ranged from 5.14 to 30.4 mg/m^2 (Figure 5a). There was no clear relationship between the integrated Chl-*a* and R_K (Figure 5a). The pigment data revealed that all the incubation stations were dominated by *Prochlorococcus* and *Synechococcus*, which are small cyanobacteria (Figure 6). These two genera accounted for most of the Chl-*a* (~72%). Haptophytes_8 and Haptophyts_6 together accounted for ~16% of the Chl-*a*. The biomass of these dominant groups was not significantly affected by the intrusion of Kuroshio Current water (Figure 6). The integrated bacterial abundance reached a peak of 3.3×10^{14} cells m^{-2} at an R_K of ~65% (Figure 5b), and the piecewise linear model (Figure 5b) gave a much better fit to the data than a horizontal line. ($F = 8.69$, $p = 0.001$, Table 1 and Figure 5b).

3.3. Euphotic Zone Integrated Microbial Responses to the Kuroshio Intrusion

Figures 7 and 8 show the spatial distributions of integrated microbial metabolism within the euphotic zone and their relationships with R_K. For oxygen-based metabolism, the integrated GPP and NCP exhibited more pronounced spatial variability (Figures 7a and 7c). The GPPs varied between 45.6 mmol O_2 m^{-2}/day at station A10 and 177 mmol O_2 m^{-2}/day at station A3 (Figure 7a). The graph of GPP versus R_K revealed a unimodal relationship between GPP and R_K, with a maximum GPP at an R_K of about 50% (Figure 8a). Because the NCP was derived from the GPP subtracted by constant CR, the spatial pattern of the integrated NCP was similar to that of GPP (Figure 7c). The NCPs were positive at R_K values of 40–80% with the maximum (76.6 mmol O_2 m^{-2}/day) observed at $R_K = 52\%$ (Figures 8a and 8c). In the region where R_K was less than 50%, the NCP tended to be negative (Figures 7c and 8c). The piecewise linear model was a significant improvement over a horizontal line in both cases ($p = 0.008$). The spatial distribution of CR was less variable

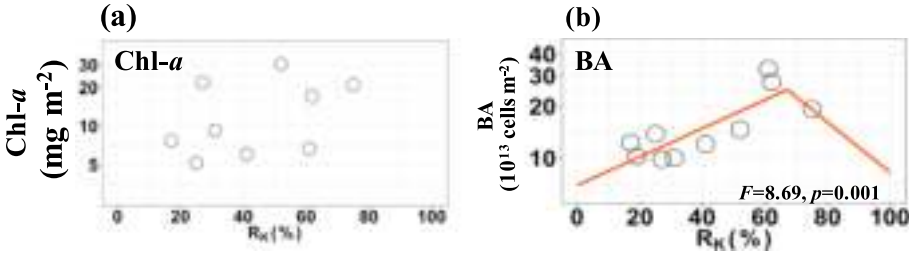

Figure 5. (a) Integrated Chlorophyll-*a* (Chl-*a*) concentration and (b) integrated bacterial abundance (BA) versus the fraction of Kuroshio intrusion in the upper 100 m (R_K). The data on the ordinate are plotted on a logarithmic scale. The F and p represent the F statistic and its associated type I error rate, respectively.

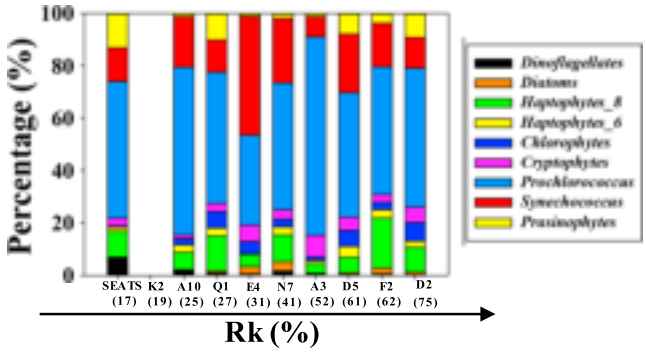

Figure 6. The contributions of different phytoplankton groups to the total integrated Chl-*a* concentration in the euphotic zone. The numbers in the bracket indicate the fraction of Kuroshio intrusion in the upper 100 m (R_K). The sample for high-performance liquid chromatography analysis at station K2 was missing.

than that of GPP; its mean value was 100 mmol O_2 m^{-2}/day (Figure 7b). The piecewise linear model did not provide a significantly better description of the CR data than a horizontal line ($F = 3.7$, $p = 0.078$, Figure 8b and Table 1).

The integrated BP was positively correlated with R_K from 12.8 mg C m^{-2}/day at an R_K of 17% (station SEATS) to a peak value of 38.6 mg C m^{-2}/day at an R_K of 60% (station D5, Figures 7d and 8d). The two BPs at higher R_K values were both less than 25 mg C m^{-2}/day (Figure 8d). The piecewise linear model (Figure 8d) gave a much better fit to the BP data than a horizontal line ($F = 6.54$, $p = 0.003$, Table 1). The BR determined by INT reduction rates contributed 30–60% of CR on average, with a range of 41.0–85.4 mmol O_2 m^{-3}/day (Figure 7e). The spatial distribution of BR was relatively homogenous (Figure 7e), and a piecewise linear model did not provide a better description than a horizontal line ($F = 1.3$, $p = 0.320$, Table 1 and Figure 8e). The calculated BGE varied between 12% and 24% (Figure 8f). The maximum of BP at an R_K of ~60% and the relatively constant BR resulted in the highest BGEs (20–24%) at an R_K of ~60% (Figure 8f). The piecewise linear model was an improvement over a horizontal line at $p = 0.042$ (Table 1).

3.4. The Estimated Amount of Nitrogen Released by the Bacterial Catabolism and the Peak of Inorganic Nitrogen Concentration in the Seawater at $R_K = 60\%$

Table 2 shows the anomaly of bacterial nitrogen-based biomass, inorganic nitrogen concentration ($NH_4^+ + NO_3^-$), and the estimated amount of nitrogen released by the bacterial catabolism at $R_K = 60\%$. The extrapolated values of BA and inorganic nitrogen at $R_K = 0\%$ and 100% (Table 2 and Figures 3 and 4) indicated that the Kuroshio ($R_K = 100\%$) had higher bacterial abundance but a lower $NH_4^+ + NO_3^-$ concentration than the NSCS ($R_K = 0\%$). At $R_K = 60\%$, the anomalies of BA, BB_N, and $NH_4^+ + NO_3^-$ were 2.49×10^{14} cells m^{-2}, 108 mmol N m^{-2}, and 276 mmol N m^{-2}, respectively (Table 2). Our estimates of BGE (20–24% at $R_K = 60\%$) imply that bacterial catabolism could release 249–332 mmol N m^{-2} (Table 2 and Figure 8f).

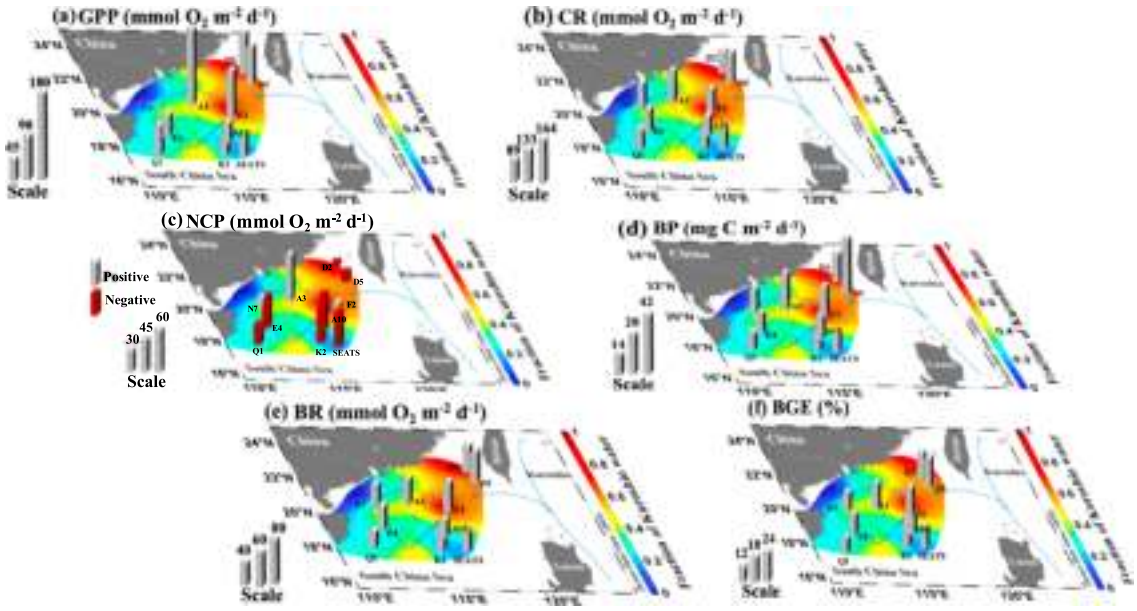

Figure 7. Spatial distributions of the integrated (a) gross primary production (GPP), (b) CR, (c) net community production (NCP), (d) bacterial production (BP), (e) bacterial respiration (BR), and (f) bacterial growth efficiency (BGE) within the euphotic zone in the NSCS during the cruise.

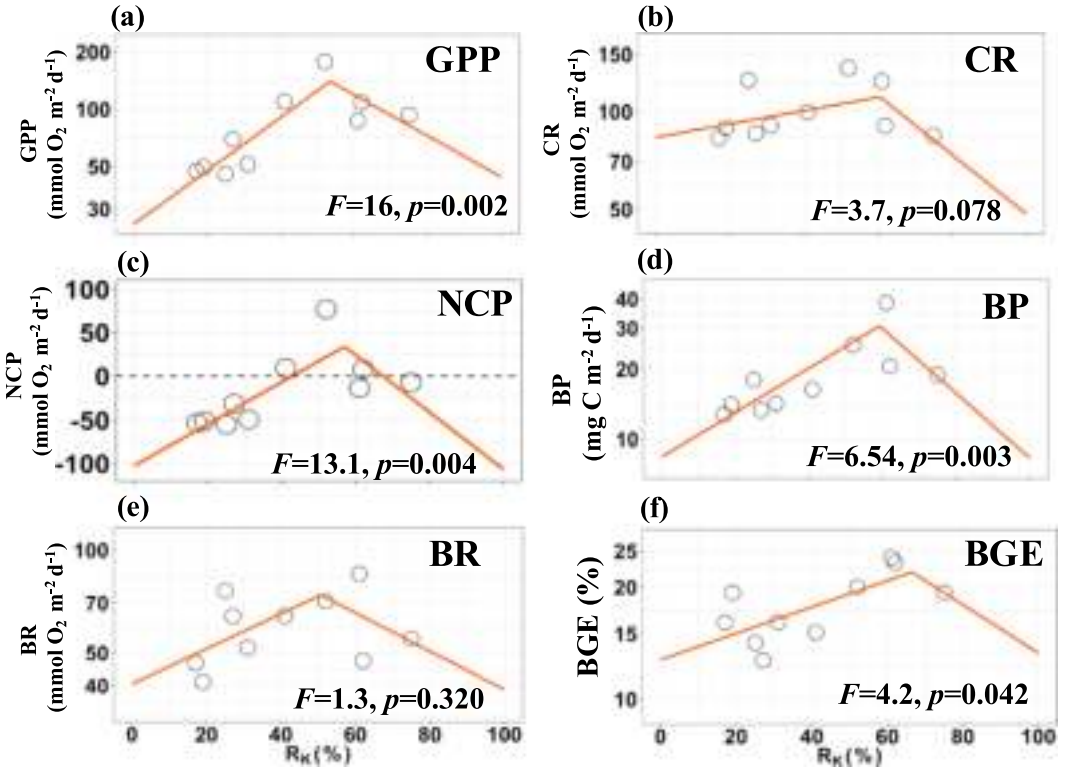

Figure 8. The relationships between the integrated metabolic rates versus the fraction of Kuroshio intrusion in the upper 100 m (R_K). The F and p represent the F statistic and its associated Type I error rate, respectively. The data on the ordinate are plotted on a logarithmic scale (except for NCP). GPP: gross primary production; CR: community respiration; NCP: net community production; BP: bacterial production; BR: bacterial respiration; BGE: bacterial growth efficiency.

4. Discussion

4.1. Quantification of Kuroshio Intrusion

Detailed information about the Kuroshio intrusion during the time of our sampling has been provided by Xu et al. (2018). Overall, the Kuroshio water invaded into the NSCS basin from the east to the west through the Luzon Strait (Figure 3b). The hydrographic features of our sampling stations, all of which fell within the θ-S boundaries of the two reference stations (Figure 3a), were consistent with our selection of these two end-members to calculate R_K values. In this mixing model, we assumed the effects of diapycnal mixing to be

Table 2
Estimates in the Anomaly of Bacterial Nitrogen-Based Biomass and Inorganic Nitrogen Concentration in the Seawater at R_K = 60%

Variable	R_K = 0% (NSCS)	R_K = 100% (Kuroshio)	R_K = 60% (Theoretical estimates)	R_K = 60% (in situ measurement)	Anomaly at R_K = 60% (Δ)
BA (10^{13} cells m^{-2})	6.6	8.1	7.5	32.4	24.9
BB_N (mmol N m^{-2})	22	27	25	108	83
$NH_4^+ + NO_3^-$ (mmol N m^{-2})	10.2	5.0	7.1	276	269
BC_N (mmol N m^{-2})	-	-	-	-	249–332

Note. The bacterial nitrogen biomass (BB_N) was estimated from the bacterial abundance (BA) multiplied by the empirical bacterial carbon content (20 fg C $cell^{-1}$; Fukuda et al., 1998) and the atomic N:C elemental ratio (1:5) for bacteria (Goldman et al., 1987). BC_N: the estimated amount of nitrogen released by bacterial catabolism.

negligible compared to isopycnal mixing. Du et al. (2013) have used Ca^{2+} as a conservative tracer to validate the model and found that the results predicted from the mixing model agreed well with field observations of Ca^{2+} concentrations in the upper 100 m of the NSCS basin. The threefold higher estimates of nutrient and total organic carbon fluxes from isopycnal mixing compared to diapycnal mixing further support the dominant role of isopycnal mixing (Du et al., 2013; Wu et al., 2015). In this study, a clearly unimodal pattern of metabolic rates versus R_K was observed, with the maximum of metabolic rates occurring at an R_K of 0.5 or 0.6 (Figures 7 and 8). The significant monotonic decrease of metabolic rates, with the exception of BR and CR, on both sides of the optimum R_K (Figure 8 and Table 1) confirmed our hypothesis that there was an *optimum* R_K for enhancement of microbial metabolism. However, the optimum R_K differed between autotrophs and heterotrophs. The optimum R_K was 50% for autotrophic metabolism (i.e., GPP and NCP) and 60% for heterotrophic bacterial variables (i.e., BA, BP, and BGE, Figure 8 and Table 1). The mechanism responsible for the optimum R_K of these metrics presumably reflects the best combination of DOM (from the Kuroshio) and inorganic nutrients (from the NSCS) in the case of the heterotrophic bacteria versus inorganic nutrients (from the NSCS and from remineralization of DOM) in the case of the autotrophic community (see the following discussion). The different optimum R_K values for the different parameters are also related to the sensitivity and limit of detection of our incubation methodology to quantify the effects of the Kuroshio intrusion on metabolic rates. However, it is worth noting that because the R_K estimated from the two-end-member mixing model is a function of the end-members, the R_K would not necessarily indicate the absolute contribution of Kuroshio water. Strictly speaking, the R_K that we calculated indicated the relative contribution of water from station P4 (Figure 3), which is located in the main path of the Kuroshio Current (so-call *typical Kuroshio*). The calculated Kuroshio contribution would have increased had we chosen a NSCS station farther to the south with more distinctive hydrography for the NSCS end-member. Therefore, the optimum R_K observed in our present study is still a statistical tool that facilitates describing the relative contribution of Kuroshio Current water and enables comparisons of the responses of different variables. Further study is clearly needed to interpret the Kuroshio signal in a more meaningful way, especially for purposes of tracking DOM composition along the pathway of the Kuroshio intrusion.

Despite the fact that some of our incubation stations were closer to land than others, the cyclonic circulation induced by the northeast monsoon effectively isolated the influence of land runoff (Figure 1), and hence, our study region was oligotrophic. Similar to major oligotrophic basins, all of our sampling stations were characterized by community structures dominated by picophytoplankton and low nitrate concentrations in the upper water column (Figure 6). Hence, we were able to examine the effects of the intrusion of Kuroshio water in the absence of other sources of horizontal variability. In the following paragraph, we discuss the impact of the intrusion of the Kuroshio Current on autotrophic and heterotrophic microbial production and microbial community composition.

4.2. Response of Heterotrophic Bacteria

We observed a significant increase of bacterial growth and activity, reflected by higher bacterial abundance (Figure 5a) and BP (Figure 7d) at R_K = ~60%. A previous study has also reported a high abundance of heterotrophic bacteria in the Kuroshio-affected region of the NSCS (Li et al., 2017). The statistical significance of the fit of the piecewise liner model to the data in the cases of BA, BP, and BGE (Figures 5b, 8d, and 8f, respectively) suggests that the Kuroshio and NSCS stimulated bacterial production in a complementary manner. The factors contributing to the enhancement of bacterial activity may have been complex. On the one hand, the enhancement of bacterial metabolism may have resulted from the stimulation of primary production, which is commonly considered to be the main source of organic carbon for bacteria (Hoppe et al., 2002; Morán et al., 2002). If that were the case, we would have expected a good correlation between the GPP and BP. The weak relationship between the two variables ($r = 0.38$, $p = 0.268$) suggests that factors other than GPP contributed to the stimulation of BP. Parallel with the maximum value of bacterial metrics at R_K = 60%, there was a similar pattern of NO_3^- concentrations versus R_K with a maximum at R_K = 50% (Figure 4a). There was no relationship between the integrated NH_4^+ concentrations and R_K (Figures 4 and 8). Ammonium is preferentially taken up by microbes versus nitrate (Pennock & Sharp, 1994) and is thus characterized by a short residence time in seawater. The rapid consumption of NH_4^+ by microbes draws down NH_4^+ concentrations to more-or-less uniformly low levels. Some high NH_4^+ concentrations observed around R_K = 50–60% (Figure 4) may reflect ammonification of DON and/or excretion by microzooplankton.

The peak of inorganic nitrogen at R_K = 50% is inconsistent with a simple mixing model and implies that there was a source of nitrate (Table 2). Interesting, we found that the estimated amount of inorganic nitrogen (249–332 mmol N m^{-2}) made available by bacterial catabolism was comparable to the difference between the measured areal inorganic nitrogen concentration (276 mmol N m^{-2}) and the areal concentration expected based on simple mixing of Kuroshio and NSCS water (7 mmol N m^{-2}; Table 2). This similarity indicates that the mechanism that stimulated the bacteria was very likely the DOM transported by the Kuroshio. If this DOM was easily exploited by the specific bacteria in the NSCS, its catabolism could have released inorganic nitrogen into the surrounding water via bacteria-mediated ammonification. The accumulation of DOM in the Kuroshio might have been due to the extremely low inorganic nutrient concentrations in the Kuroshio (Du et al., 2013), which would effectively retard organic matter decomposition (Carlson et al., 2011; Shiah et al., 1998; van Wambeke et al., 2016). Nutrient concentrations in the NSCS are relatively high compared to the Kuroshio (Du et al., 2013). During the mixing of Kuroshio and NSCS water, the former provides DOM, and the latter provides inorganic nutrients. We hypothesize that some bacteria were able to exploit this admixture and, in the process of metabolizing the DOM, released inorganic nitrogen. The DOM in the Kuroshio may therefore be exploited by bacteria that take advantage of the availability of inorganic nutrients provided by the SCS water. This scenario is consistent with the results of two nutrient enrichment experiments conducted in the adjacent western Pacific Ocean (Liu et al., 2014; Shiah et al., 1998). Those experiments documented an increased rate of DOC decomposition and an increase of bacterial activity after the addition of inorganic nutrients.

Unlike the relationship between BP and R_K, BR remained relatively constant across the range of R_K values (Figures 7e and 8e). This constancy of BR is consistent with the earlier empirical analysis by López-Urrutia and Morán (2007). They found a relatively weak or insignificant relationship between BR and organic matter availability in the upper 200 m of the ocean, unlike the relationship between BP and DOC. Under resource-depleted conditions, the energy provided by bacterial metabolism (i.e., respiration) is allocated to satisfy maintenance metabolic costs (Carlson et al., 2007; del Giorgio & Cole, 1998). When resources are less limiting, the metabolic energy is allocated more for biomass production, as reflected by the significant elevation of BGE at R_K = ~60% (Figure 8f).

4.3. Response of Autotrophic Metabolism

At stations with R_K < 30%, the integrated GPP averaged 53 ± 5.5 mmol O_2 m^{-2}/day (Figure 7a), very close to the mean value (51 ± 10 mmol O_2 m^{-2}/day) determined by the same methodology in the NSCS basin during the summer (Wang et al., 2014). Along the path of the Kuroshio intrusion, we observed a response of GPP around R_K = 50% followed by responses from heterotrophic bacteria at R_K = 60% (Figure 8). This pattern suggests that the first effect of mixing Kuroshio water with NSCS water was a stimulation of bacterial activity, and subsequently, there was a stimulation of phytoplankton activity. The maximum GPP at the optimum R_K was almost 4 times the lowest GPP at R_K = 25%. However, the absence of a corresponding relationship both in the case of Chl-*a* and community structure (Figures 5a and 6) implied that the response of autotrophs to the elevated nitrate concentration near R_K = 50% was a dramatic increase in growth rate but very little change in biomass. This raises a question of how phytoplankton biomass and production are controlled in this system. Based on the estimates from the piecewise linear model, the areal nitrate concentrations at NSCS (R_K = 0%) was about 10.5 mmol/m^2, roughly twice the amount of nitrate in the Kuroshio (4.5 mmol/m^2 at R_K = 0%, Figure 4a). These areal concentrations translate to average concentrations of 105 and 45 nM in the euphotic zone, which are small compared to the half-saturation constant for growth of *Thalassiosira pseudonana* (816 nM) estimated by Garside and Glover (1991). Therefore, the growth rates of the phytoplankton populations in both the NSCS and Kuroshio were limited by inorganic nitrogen. The areal concentration of phytoplankton nitrogen can be estimated by multiplying the average areal Chl-*a* concentration (30.4 mg/m^2) by an assumed C:Chl-*a* ratio of 50 g/g (Strickland & Parsons, 1972) and dividing by an assumed C:N ratio of 5.68 g/g (Redfield, 1958). This calculation gives an areal phytoplankton nitrogen concentration of 268 mg/m^2 or 19.1 mmol/m^2, which is only 8% of the peak nitrate concentration of 239 mmol/m^2 (Figure 4a). The implication is that the enhancement of GPP near R_K = 50% was associated with a biomass of phytoplankton that was a small fraction of the biomass that could have been produced from the elevation of inorganic nitrogen. Previous studies in upwelling systems have shown that the abundance of large phytoplankton, particularly diatoms, increases in response to an influx of

inorganic nutrients (Lundry et al., 1997). Grazing by macrozooplankton has a limited effect on large diatoms in such cases because macrozooplankton have relatively long generation times (Lundry et al., 1997). The absence of a response of large phytoplankton to nitrogen enrichment in this study suggests that a nutrient other than nitrogen may have been limiting. A recent study has indicated that phytoplankton production in the South China Sea basin is colimited by nitrogen and iron based on observations of a diel cycle of phytoplankton nutritional status assayed by a fluorescence signal (Xie et al., 2018). The iron concentration in the upper layer of the NSCS basin during the summer is about 0.2–0.3 nM (Wu et al., 2003), which is low enough to lead to iron stress for phytoplankton (Sedwick et al., 2000). The Kuroshio is an extension of the North Equatorial Current, where iron is limiting (Behrenfeld et al., 1996). Although there has been no report to date of iron concentrations in the subtropical Kuroshio Current, it is reasonable to infer that the iron concentration might be lower in the Kuroshio than in the NSCS because it is an extension of the North Equatorial Current and is farther from an allochthonous iron source (i.e., Asian dust deposition; Wang et al., 2012) than the NSCS. We hypothesize that low iron concentrations probably limited the growth of large phytoplankton under the nitrate-replete conditions at R_K values near 50%. Small phytoplankton, however, are better able to exploit low iron concentrations because of their relatively large surface-to-volume ratios. Hence, their growth rates could increase in response to the increase of nitrate concentrations. However, the microzooplankton that graze *Synechococcus* and *Prochlorococcus* have short generation times and thus can effectively prevent picophytoplankton such as *Synechococcus* and *Prochlorococcus* from increasing in numbers (Lundry et al., 1997). The increase in picophytoplankton growth rates at $R_K = 50\%$ might thus be counterbalanced by the accompanying increase in the grazing pressure, the result being no change in biomass. Furthermore, increased grazing is associated with an increase in the rate of nutrient recycling, which in turn sustains the rapid growth rate of the picophytoplankton.

4.4. Responses of NCP

The simultaneous changes of autotrophic and heterotrophic metabolism with changes of R_K resulted in a significant elevation of NCP at $R_K = \sim 50\%$ (Figures 7c and 8c). During the summer, strong stratification in the upper water column minimizes the supply of nutrients from deeper water and hence reduces production in the euphotic zone (Lee Chen, 2005; Ning et al., 2004; Wong et al., 2007). As a result, export production in the NSCS during this period is low (Cai et al., 2015; Lee Chen, 2005; Liu & Chai, 2009). NCP usually tends to be negative based on oxygen mass balance models (Huang et al., 2018), dissolved inorganic carbon budgets (Chou et al., 2006), and our present incubation results (Figure 7c). However, NCP near $R_K = \sim 50\%$ was positive (Figure 7c). A positive NCP implies that organic carbon is available for export (Ducklow & Doney, 2013). The Kuroshio intrusion-associated shift of metabolic state emphasizes the impact of currents on microbial metabolism and overall carbon cycling in the oligotrophic waters of the NSCS basin.

Based on the foregoing results and discussion, we propose a hypothetical mechanism of how transport of Kuroshio water impacts biogeochemical processes in the NSCS basin (Figure 9): Compared to the NSCS, the Kuroshio water is DOM rich but deficient in inorganic nutrients. We hypothesize that bacterial utilization of DOC in the Kuroshio Current is constrained by the low inorganic nutrient concentrations in the Kuroshio. The intrusion of the Kuroshio into the NSCS basin leads to the admixture of DOC provided by the Kuroshio Current and inorganic nutrients injected by the NSCS. Such mixing processes potentially create a better scenario for some bacteria to exploit and metabolize the DOC. Therefore, the DOC transferred by the Kuroshio intrusion acts as a new carbon source to stimulate the bacterial activity. The enhanced bacterial activity releases nitrogen during remineralization of DOM. The impact of this newly produced inorganic nitrogen is profound, particularly in a nitrogen-limited ecosystem such as the NSCS basin. On the one hand, the generation of new inorganic nitrogen associated with the Kuroshio intrusion would directly stimulate local phytoplankton primary production and export production by extension. On the other hand, the source of this nitrogen differs from the conventional allochthonous nitrogen that supports export production in the oligotrophic ocean: vertical diffusion (Du et al., 2017), nitrogen fixation (Karl & Letelier, 2008), and atmospheric deposition (Duce et al., 2008). This additional nitrogen is inferred to originate partly from the transfer of organic matter by the Kuroshio Current intrusion and then decomposition into inorganic nitrogen by bacterial activity. Finally, this new nitrogen source will serve as another mechanism to fuel export production and enhance the ability of carbon sequestration in the NSCS basin. This unique mechanism provides

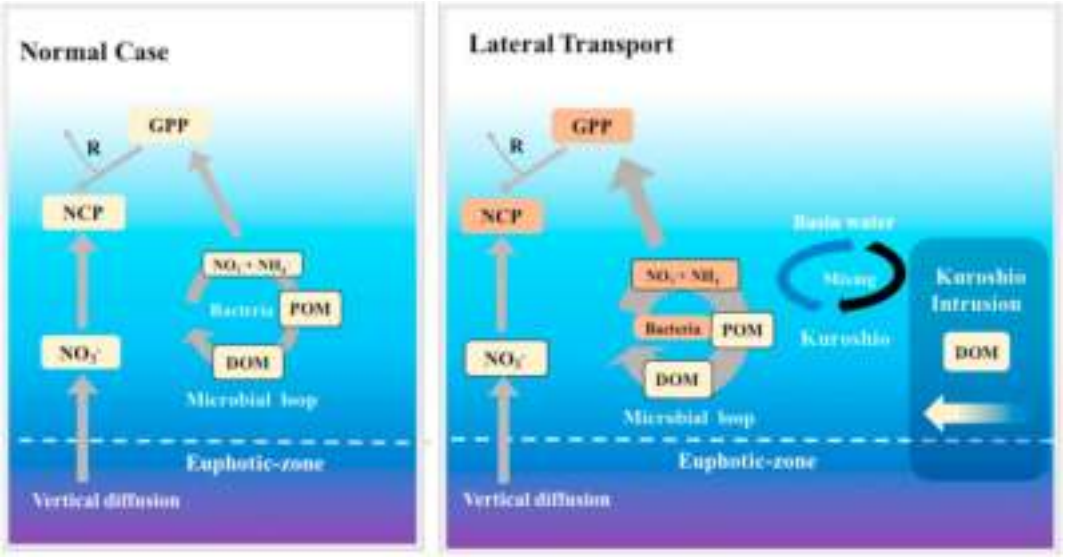

Figure 9. A schematic demonstrating the possible mechanisms responsible for the impacts associated with the intrusion of Kuroshio water on biogeochemical processes in the NSCS basin. DOM: dissolved organic matter. GPP: gross primary production. R: respiration; NCP: net community production; POM: particulate organic matter.

more insight into the impact of horizontal currents in the carbon and nitrogen cycle on a regional scale and further broadens our knowledge of the pathways that sustain export production.

5. Conclusion

Overall, the simultaneous responses of autotrophic and heterotrophic activities confirmed the importance of transport of the Kuroshio Current water on microbial community metabolism and biogeochemical processes in the oligotrophic NSCS basin. The statistically negative correlations between the metabolic rates and the absolute value of the deviation of the R_K from the optimum fraction suggest a unimodal impact of the mixture processes in stimulating the microbial metabolism. In other words, there is an *optimum ratio*. The observed increase in the nitrogen concentration and export production (NCP in this study) along with the Kuroshio intrusion provided insight into this unique driver of export production in a nutrient-limited system by new nitrogen generated from the intrusion of a current. Our study therefore provides motivation for more accurate quantification of the impact of Kuroshio intrusion on the regional carbon cycle by a combination of a hydrodynamic model and field observations, including seasonal DOC concentrations, nutrient budgets, and export production. Projected climate change scenarios indicate that there will be greater thermal stratification in the upper ocean (Bopp et al., 2013; Fu et al., 2016). Hence, advection will probably become more important relative to vertical mixing in modulating marine biogeochemical processes in the coming decades.

Acknowledgments
This study was supported by grants from the National Key Research and Development Program of China (2016YFA0601201), the China NSF Projects (41890803 and U1805241), and partially supported by the starter grant from University of Strathclyde (to B. Chen). All of the phytoplankton community structure and metabolic rates data are available in the supporting information, and please contact Dr. Huang (bqhuang@xmu. edu.cn) if any questions. And the nutrients concentration data could be acquired from the supporting information of Xu et al. (2018, https://doi.org/10.1029/2018GL077896). We also acknowledged the crew in R/V *Dongfanghong II* at the University of Ocean, China. We would like to thank Dr. Hu JianYu for providing the CTD data. This study also benefited from the discussion with Dr. Xu and Dr. Kao Shuji at Xiamen University. The authors declare no conflict of interests.

References

Abell, J., Emerson, S., & Renaud, P. (2000). Distributions of TOP, TON and TOC in the North Pacific subtropical gyre: Implications for nutrient supply in the surface ocean and remineralization in the upper thermocline. *Journal of Marine Research*, *58*(2), 203–222. https://doi.org/10.1357/002224000321511142

Azam, F., Fenchel, T., Field, J. G., Gray, J. S., Meyerreil, L. A., & Thingstad, F. (1983). The ecological role of water-column microbes in the sea. *Marine Ecology Progress Series*, *10*(3), 257–263. https://doi.org/10.3354/meps010257

Behrenfeld, M. J., Bale, A. J., Kolber, Z. S., Aiken, J., & Falkowski, P. G. (1996). Confirmation of iron limitation of phytoplankton photosynthesis in the equatorial Pacific Ocean. *Nature*, *383*(6600), 508–511. https://doi.org/10.1038/383508a0

Bopp, L., Resplandy, L., Orr, J. C., & Doney, S. C. (2013). Multiple stressors of ocean ecosystems in the 21st century: Projections with CMIP5 models. *Biogeosciences*, *10*(10), 6225–6245. https://doi.org/10.5194/bg-10-6225-2013

Bronk, D. A., See, J. H., Bradley, P., & Killberg, L. (2007). DON as a source of bioavailable nitrogen for phytoplankton. *Biogeosciences 4* (3), 283–296. https://doi.org/10.5194/bg-4-283-2007

Cai, P. H., Zhao, D. C., Wang, L., Huang, B. Q., & Dai, M. H. (2015). Role of particle stock and phytoplankton community structure in regulating particulate organic carbon export in a large marginal sea. *Journal of Geophysical Research: Oceans*, *120*, 2063–2095. https://doi.org/10.1002/2014JC010432

Carlson, C. A., Giorgio, P. A. D., & Herndl, G. J. (2007). Microbes and the dissipation of energy and respiration: From cells to ecosystems. *Oceanography*, *20*(2), 89–100. https://doi.org/10.5670/oceanog.2007.52

Carlson, C. A., Hansell, D. A., & Tamburini, C. (2011). DOC persistence and its fate after export within the ocean interior. In N. Jiao, F. Azam, & S. Sanders (Eds.), *Microbial Carbon Pump in the Ocean*, (pp. 57–59). Washington, DC: AAAS.

Chou, W. C., Chen, Y. L. L., Sheu, D. D., Shih, Y.-Y., Han, C.-A., Cho, C. L., et al. (2006). Estimated net community production during the summertime at the SEATS time-series study site, northern South China Sea: Implications for nitrogen fixation. *Geophysical Research Letters*, *33*, L22610. https://doi.org/10.1029/2005gl025365

Core, T. R. (2014), A language and environment for statistical computing, R foundation for statistical computing, Vienna, Austria., edited.

Dai, M., Cao, Z., Guo, X., Zhai, W., Liu, Z., Yin, Z., et al. (2013). Why are some marginal seas sources of atmospheric CO_2? *Geophysical Research Letters*, *40*, 2154–2158. https://doi.org/10.1002/grl.50390

del Giorgio, P. A., & Cole, J. J. (1998). Bacterial growth efficiency in natural aquatic systems. *Annual Review of Ecology, Evolution, and Systematics*, *29*(1), 503–541. https://doi.org/10.1146/annurev.ecolsys.29.1.503

del Giorgio, P. A., Cole, J. J., & Cimbleris, A. (1997). Respiration rates in bacteria exceed phytoplankton production in unproductive aquatic systems. *Nature*, *385*(6612), 148–151. https://doi.org/10.1038/385148a0

Du, C., Liu, Z., Dai, M., Kao, S. J., Cao, Z., Zhang, Y., et al. (2013). Impact of the Kuroshio intrusion on the nutrient inventory in the upper northern South China Sea: Insights from an isopycnal mixing model. *Biogeosciences*, *10*(10), 6419–6432. https://doi.org/10.5194/bg-10-6419-2013

Du, C. J., Liu, Z. Y., Kao, S. J., & Dai, M. H. (2017). Diapycnal fluxes of nutrients in an oligotrophic oceanic regime: The South China Sea. *Geophysical Research Letters*, *44*, 11,510–11,518. https://doi.org/10.1002/2017gl074921

Duce, R. A., LaRoche, J., Altieri, K., Arrigo, K. R., Baker, A. R., Capone, D. G., et al. (2008). Impacts of atmospheric anthropogenic nitrogen on the open ocean. *Science*, *320*(5878), 893–897. https://doi.org/10.1126/science.1150369

Ducklow, H. W. (1999). The bacterial component of the oceanic euphotic zone. *FEMS Microbiology Ecology*, *30*(1), 1–10. https://doi.org/10.1111/j.1574-6941.1999.tb00630.x

Ducklow, H. W., & Doney, S. C. (2013). What is the metabolic state of the oligotrophic ocean? A debate. *Annual Review of Marine Science*, *5*(1), 525–533. https://doi.org/10.1146/annurev-marine-121211-172331

Falkowski, P. G., Laws, E. A., Barber, R. T., & Murray, J. W. (2003). In M. J. R. Ifasham (Ed.), *Phytoplankton and their role in primary, new, and export production*, *Ocean Biogeochemistry. Global Change—The IGBP Series (closed)*, (pp. 99–121). Berlin, Heidelberg: Springer. https://doi.org/10.1007/978-3-642-55844-3_5

Fang, G., Wang, Y., Wei, Z., Fang, Y., Qiao, F., & Hu, X. (2009). Interocean circulation and heat and freshwater budgets of the South China Sea based on a numerical model. *Dynamics of Atmospheres and Oceans*, *47*(1–3), 55–72. https://doi.org/10.1016/j.dynatmoce.2008.09.003

Fontes, M. L. S., Berri, A., Carvalho, M., Fonseca, A. L. O., Antônio, R. V., & Freire, A. S. (2018). Bacterioplankton abundance and biomass stimulated by water masses intrusions over the Southern Brazilian Shelf (between 25°57'S and 29°24'S). *Continental Shelf Research*, *164*, 28–36. https://doi.org/10.1016/j.csr.2018.05.003

Fu, W., Randerson, J., & Moore, J. K. (2016). Climate change impacts on net primary production (NPP) and export production (EP) regulated by increasing stratification and phytoplankton community structure in CMIP5 models. *Biogeosciences Discussions*, *12*(15), –12,851, 12,897. https://doi.org/10.5194/bgd-12-12851-2015

Fukuda, R., Ogawa, H., Nagata, T., & Koike, I. (1998). Direct determination of carbon and nitrogen contents of natural bacterial assemblages in marine environments. *Applied and Environmental Microbiology*, *64*(9), 3352–3358.

Furuya, K., & Harada, K. (1995). An automated precise Winkler titration for determining dissolved oxygen on board ship. *Journal of Oceanography*, *51*(3), 375–383. https://doi.org/10.1007/bf02285173

García-Martín, E. E., Aranguren-Gassis, M., Hartmann, M., Zubkov, M. V., & Serret, P. (2017). Contribution of bacterial respiration to plankton respiration from 50°N to 44°S in the Atlantic Ocean. *Progress in Oceanography*, *158*, 99–108. https://doi.org/10.1016/j.pocean.2016.11.006

Garside, C., & Glover, H. E. (1991). Chemiluminescent measurements of nitrate kinetics: I. Thalassiosira pseudonana (clone 3H) and neriticassemblages. *Journal of Plankton Research*. *13*(1), 5–19. https://doi.org/10.1093/oxfordjournals.plankt.a042370

Gist, N., Serret, P., Woodward, E. M. S., Chamberlain, K., & Robinson, C. (2009). Seasonal and spatial variability in plankton production and respiration in the subtropical gyres of the Atlantic Ocean. *Deep Sea Research. Part II: Topical Studies in Oceanography*, *56*(15), 931–940. https://doi.org/10.1016/j.dsr2.2008.10.035

Goldman, J. C., Caron, D. A., & Dennett, M. R. (1987). Regulation of gross growth efficiency and ammonium regeneration in bacteria by substrate C:N ratio. *Limnology and Oceanography*, *32*(6), 1239–1252. https://doi.org/10.4319/lo.1987.32.6.1239

Gong, G.-C., Wen, Y.-H., Wang, B.-W., & Liu, G.-J. (2003). Seasonal variation of chlorophyll *a* concentration, primary production and environmental conditions in the subtropical East China Sea. *Deep Sea Research. Part II: Topical Studies in Oceanography*, *50*(6-7), 1219–1236. https://doi.org/10.1016/s0967-0645(03)00019-5

Han, A., Dai, M., Kao, S.-J., Gan, J., Li, Q., Wang, L., et al. (2012). Nutrient dynamics and biological consumption in a large continental shelf system under the influence of both a river plume and coastal upwelling. *Limnology and Oceanography*, *57*(2), 486–502. https://doi.org/10.4319/lo.2012.57.2.0486

Hedges, J. I., Baldock, J. A., Gélinas, Y., Lee, C., Peterson, M. L., & Wakeham, S. G. (2002). The biochemical and elemental compositions of marine plankton: A NMR perspective. *Marine Chemistry*, *78*(1), 47–63. https://doi.org/10.1016/S0304-4203(02)00009-9

Hoppe, H. G., Gocke, K., Koppe, R., & Begler, C. (2002). Bacterial growth and primary production along a north-south transect of the Atlantic Ocean. *Nature*, *416*(6877), 168–171. https://doi.org/10.1038/416168a

Hu, D., Wu, L., Cai, W., Gupta, A. S., Ganachaud, A., Qiu, B., et al. (2015). Pacific western boundary currents and their roles in climate. *Nature*, *522*(7556), 299–308. https://doi.org/10.1038/nature14504

Hu, J., Kawamura, H., Hong, H., & Qi, Y. (2000). A review on the currents in the South China Sea: Seasonal circulation, South China Sea warm current and Kuroshio intrusion. *Journal of Oceanography*, *56*(6), 607–624. https://doi.org/10.1023/a:1011117531252

Huang, Y., Chen, B., Huang, B., Zhou, H., & Yuan, Y. (2019). Potential overestimation of community respiration in the western Pacific boundary ocean: What causes the putative net heterotrophy in oligotrophic systems? *Limnology and Oceanography*. https://doi.org/10.1002/lno.11179

Huang, Y., Yang, B., Chen, B., Qiu, G., Wang, H., & Huang, B. (2018). Net community production in the South China Sea Basin estimated from *in situ* O_2 measurements on an Argo profiling float. *Deep Sea Research. Part I: Oceanographic Research Papers*, *131*, 54–61. https://doi.org/10.1016/j.dsr.2017.11.002

Huthnance, J. M., Holt, J. T., & Wakelin, S. L. (2009). Deep ocean exchange with west-European shelf seas. *Ocean Science*, *5*(4), 621–634. https://doi.org/10.5194/os-5-621-2009

Jenkins, W. J., & Doney, S. C. (2003). The subtropical nutrient spiral. *Global Biogeochemical Cycles*, *17*(4), 1110. https://doi.org/10.1029/2003GB002085

Johnson, K. S., Riser, S. C., & Karl, D. M. (2010). Nitrate supply from deep to near-surface waters of the North Pacific subtropical gyre. *Nature*, *465*(7301), 1062–1065. https://doi.org/10.1038/nature09170

Karl, D. M., & Letelier, R. M. (2008). Nitrogen fixation-enhanced carbon sequestration in low nitrate, low chlorophyll seascapes. *Marine Ecology Progress Series*, *364*, 257–268. https://doi.org/10.3354/meps07547

Kirchman, D. (2001). Measuring bacterial biomass production and growth rates from leucine incorporation in natural aquatic environments. *Methods in Microbiology*, *30*, 227–237. https://doi.org/10.1016/S0580-9517(01)30047-8

Laws, E. A. (1991). Photosynthetic quotients, new production and net community production in the open ocean. *Deep Sea Research Part I: Oceanographic Research Papers*, *38*(1), 143–167. https://doi.org/10.1016/0198-0149(91)90059-O

Lee Chen, Y. (2005). Spatial and seasonal variations of nitrate-based new production and primary production in the South China Sea. *Deep Sea Research.Part I: Oceanographic Research Papers*, *52*(2), 319–340. https://doi.org/10.1016/j.dsr.2004.11.001

Lee Chen, Y., & Chen, H.-Y. (2006). Seasonal dynamics of primary and new production in the northern South China Sea: The significance of river discharge and nutrient advection. *Deep Sea Research. Part I: Oceanographic Research Papers*, *53*(6), 971–986. https://doi.org/10.1016/j.dsr.2006.02.005

Lee Chen, Y., Chen, H.-Y., Tuo, S.-H., & Ohki, K. (2008). Seasonal dynamics of new production from Trichodesmium N_2 fixation and nitrate uptake in the upstream Kuroshio and South China Sea basin. *Limnology and Oceanography*, *53*(5), 1705–1721. https://doi.org/10.4319/lo.2008.53.5.1705

Letscher, R. T., Primeau, F., & Moore, J. K. (2016). Nutrient budgets in the subtropical ocean gyres dominated by transport. *Nature Geoscience*, *9*(11), 815–819. https://doi.org/10.1038/ngeo2812

Li, J., Jiang, X., Li, G., Jing, Z., Zhou, L., Ke, Z., & Tan, Y. (2017). Distribution of picoplankton in the northeastern South China Sea with special reference to the effects of the Kuroshio intrusion and the associated mesoscale eddies. *Science of the Total Environment*, *589*, 1–10. https://doi.org/10.1016/j.scitotenv.2017.02.208

Liu, G., & Chai, F. (2009). Seasonal and interannual variability of primary and export production in the South China Sea: A three-dimensional physical-biogeochemical model study. *ICES Journal of Marine Science*, *66*(2), 420–431. https://doi.org/10.1093/icesjms/fsn219

Liu, J., Jiao, N., & Tang, K. (2014). An experimental study on the effects of nutrient enrichment on organic carbon persistence in the western Pacific oligotrophic gyre. *Biogeosciences*, *11*(18), 5115–5122. https://doi.org/10.5194/bg-11-5115-2014

Liu, K. K., Chao, S. Y., Shaw, P. T., Gong, G. C., Chen, C. C., & Tang, T. Y. (2002). Monsoon-forced chlorophyll distribution and primary production in the South China Sea: Observations and a numerical study. *Deep Sea Research. Part I: Oceanographic Research Papers*, *49*(8), 1387–1412. https://doi.org/10.1016/s0967-0637(02)00035-3

Liu, X., Xiao, W., Landry, M. R., Chiang, K. P., Wang, L., & Huang, B. (2016). Responses of phytoplankton communities to environmental variability in the East China Sea. *Ecosystems*, *19*(5), 832–849. https://doi.org/10.1007/s10021-016-9970-5

López-Urrutia, Á., & Morán, X. A. G. (2007). Resource limitation of bacterial production distorts the temperature dependence of oceanic carbon cycling. *Ecology*, *88*(4), 817–822. https://doi.org/10.1890/06-1641

Lozier, M. S., Dave, A. C., Palter, J. B., Gerber, L. M., & Barber, R. T. (2011). On the relationship between stratification and primary productivity in the North Atlantic. *Geophysical Research Letters*, *38*, L18609. https://doi.org/10.1029/2011GL049414

Lundry, M. R., Barber, R. T., Bidare, R. R., Chai, F., Coale, K. H., Dam, H. G., et al. (1997). Iron and grazing constraints on primary production in the central equatorial Pacific: An EqPac synthesis. *Limnology and Oceanography*, *42*(3), 405–418. https://doi.org/10.4319/lo.1997.42.3.0405

Mackey, M., Mackey, D., Higgins, H., & Wright, S. (1996). CHEMTAX—A program for estimating class abundances from chemical markers:application to HPLC measurements of phytoplankton. *Marine Ecology Progress*, *144*(1), 265–283. https://doi.org/10.3354/meps144265

Marie, D., Partensky, F., Jacquet, S., & Vaulot, D. (1997). Enumeration and cell cycle analysis of natural populations of marine picoplankton by flow cytometry using the nucleic acid stain SYBR Green I. *Applied and Environmental Microbiology*, *63*(1), 186–193.

Martínez-García, S., Fernández, E., Aranguren-Gassis, M., & Teira, E. (2009). In vivo electron transport system activity: A method to estimate respiration in natural marine microbial planktonic communities. *Limnology and Oceanography: Methods*, *7*(6), 459–469. https://doi.org/10.4319/lom.2009.7.459

Miller, J. C., & Miller, J. N. (1988). Statistics for analytical chemistry. In *Analytical and Bioanalytical Chemistry* (2nd ed., Vol. 378, pp. 1676–1677). Great Britain: Ellis Howood Limtied.

Morán, X. A., Estrada, M., Gasol, J. M., & Pedrós-Alió, C. (2002). Dissolved primary production and the strength of phytoplankton-bacterioplankton coupling in contrasting marine regions. *Microbial Ecology*, *44*(3), 217–223. https://doi.org/10.1007/s00248-002-1026-z

Nan, F., Xue, H., & Yu, F. (2015). Kuroshio intrusion into the South China Sea: A review. *Progress in Oceanography*, *137*, 314–333. https://doi.org/10.1016/j.pocean.2014.05.012

Ning, X., Chai, F., Xue, H., Cai, Y., Liu, C., & Shi, J. (2004). Physical-biological oceanographic coupling influencing phytoplankton and primary production in the South China Sea. *Journal of Geophysical Research*, *109*, C10005. https://doi.org/10.1029/2004JC002365

Oudot, C., Gerard, R., Morin, P., & Gningue, I. (1988). Precise shipboard determination of dissolved-oxygen (Winkler procedure) for productivity studies with a commercial system. *Limnology and Oceanography*, *33*(1), 146–150. https://doi.org/10.4319/lo.1988.33.1.0146

Patey, M. D., Rijkenberg, M. J. A., Statham, P. J., Stinchcombe, M. C., Achterberg, E. P., & Mowlem, M. (2008). Determination of nitrate and phosphate in seawater at nanomolar concentrations. *Trends in Analytical Chemistry*, *27*(2), 169–182. https://doi.org/10.1016/j.trac.2007.12.006

Pennock, J. R., & Sharp, J. H. (1994). Temporal alternation between light- and nutrient limitation of phytoplankton production in a coastal plain estuary. *Marine Ecology Progress Series*, *111*, 275–288. https://doi.org/10.3354/meps111275

Qiu, C., Mao, H., Yu, J., Xie, Q., Wu, J., Lian, S., & Liu, Q. (2015). Sea surface cooling in the Northern South China Sea observed using Chinese sea-wing underwater glider measurements. *Deep Sea Research. Part I: Oceanographic Research Papers*, *105*, 111–118. https://doi.org/10.1016/j.dsr.2015.08.009

Qu, T., Mitsudera, H., & Yamagata, T. (2000). Intrusion of the North Pacific waters into the South China Sea. *Journal of Geophysical Research*, *105*(C3), 6415–6424. https://doi.org/10.1029/1999JC900323

Redfield, A. C. (1958). The biological control of chemical factors in the environment. *American Scientist*, *46*(3), 230A–221A.

Reynolds, S., Mahaffey, C., Roussenov, V., & Williams, R. G. (2014). Evidence for production and transport of dissolved organic phosphorus in the eastern subtropical North Atlantic. *Global Biogeochemical Cycles*, *28*, 805–824. https://doi.org/10.1002/2013GB004801

Schlitzer, R. (2012), Ocean data view Available at odv.awi.de. Accessed November 3, 2013, edited.
Sedwick, P. N., DiTullio, G. R., & Mackey, D. J. (2000). Iron and manganese in the Ross Sea, Antarctica: Seasonal iron limitation in Antarctic shelf waters. *Journal of Geophysical Research*, *105*(C5), 11,321–11,336. https://doi.org/10.1029/2000JC000256
Shiah, F. K., Kao, S. J., & Liu, K. K. (1998). Bacterial production in the western equatorial Pacific: Implications of inorganic nutrient effects on dissolved organic Carbon accumulation and consumption. *Bulletin of Marine Science -Miami*, *62*(3), 795–808.
Shiozaki, T., Takeda, S., Itoh, S., Kodama, T., Liu, X., Hashihama, F., & Furuya, K. (2015). Why is Trichodesmium abundant in the Kuroshio? *Biogeosciences*, *12*(23), 6931–6943. https://doi.org/10.5194/bg-12-6931-2015
Siegel, D. A., Buesseler, K. O., Doney, S. C., Sailley, S. F., Behrenfeld, M. J., & Boyd, P. W. (2014). Global assessment of ocean carbon export by combining satellite observations and food-web models. *Global Biogeochemical Cycles*, *28*, 181–196. https://doi.org/10.1002/2013GB004743
Sigman, D. M., & Boyle, E. A. (2000). Glacial/interglacial variations in atmospheric carbon dioxide. *Nature*, *407*(6806), 859–869. https://doi.org/10.1038/35038000
Strickland, J. D., & Parsons, T. R. (1972). *A practical handbook of seawater analysis*, (Vol. 167, p. 310). Ottawa Canada: Fisheries Resource Board.
Tian, J., Yang, Q., & Zhao, W. (2009). Enhanced diapycnal mixing in the South China Sea. *Journal of Physical Oceanography*, *39*(12), 3191–3203. https://doi.org/10.1175/2009JPO3899.1
Tseng, C. M., Wong, G. T. F., Lin, I. I., Wu, C. R., & Liu, K. K. (2005). A unique seasonal pattern in phytoplankton biomass in low-latitude waters in the South China Sea. *Geophysical Research Letters*, *32*, L08608. https://doi.org/10.1029/2004GL022111
van Wambeke, F., Pfreundt, U., Barani, A., Berthelot, H., Moutin, T., Rodier, M., et al. (2016). Heterotrophic bacterial production and metabolic balance during the VAHINE mesocosm experiment in the New Caledonia lagoon. *Biogeosciences*, *13*(11), 3187–3202. https://doi.org/10.5194/bg-13-3187-2016
Viviani, D. A., & Church, M. J. (2017). Decoupling between bacterial production and primary production over multiple time scales in the North Pacific Subtropical Gyre. *Deep Sea Research. Part I: Oceanographic Research Papers*, *121*(1), 132–142. https://doi.org/10.1016/j.dsr.2017.01.006
Wang, L., Huang, B., Chiang, K. P., Liu, X., Chen, B., Xie, Y., et al. (2016). Physical-biological coupling in the western South China Sea: The response of phytoplankton community to a mesoscale cyclonic eddy. *PLoS ONE*, *11*(4), e0153735. https://doi.org/10.1371/journal.pone.0153735
Wang, N., Lin, W., Chen, B., & Huang, B. (2014). Metabolic states of the Taiwan Strait and the northern South China Sea in summer 2012 (In Chinese with English abstract). *Journal of Tropical Oceanography*, *33*(4), 61–68.
Wang, S.-H., Hsu, N. C., Tsay, S.-C., Lin, N.-H., Sayer, A. M., Huang, S.-J., & Lau, W. K. M. (2012). Can Asian dust trigger phytoplankton blooms in the oligotrophic northern South China Sea? *Geophysical Research Letters*, *39*, L05811. https://doi.org/10.1029/2011GL050415
Wong, G. T. F., Tseng, C. M., Wen, L. S., & Chung, S. W. (2007). Nutrient dynamics and nitrate anomaly at the SEATS station. *Deep Sea Research Part II: Topical Studies in Oceanography*, *54*(14-15), 1528–1545. https://doi.org/10.1016/j.dsr2.2007.05.011
Wu, J., Chung, S.-W., Wen, L.-S., Liu, K.-K., Chen, L., Chen, H.-Y., & Karl, D. M. (2003). Dissolved inorganic phosphorus, dissolved iron, and *Trichodesmiumin* the oligotrophic South China Sea. *Global Biogeochemical Cycles*, *17*(1), 1008. https://doi.org/10.1029/2002GB001924
Wu, K., Dai, M., Chen, J., Meng, F., Li, X., Liu, Z., et al. (2015). Dissolved organic carbon in the South China Sea and its exchange with the Western Pacific Ocean. *Deep Sea Research. Part II: Topical Studies in Oceanography*, *122*, 41–51. https://doi.org/10.1016/j.dsr2.2015.06.013
Xiao, W., Wang, L., Laws, E., Xie, Y., Chen, J., Liu, X., et al. (2018). Realized niches explain spatial gradients in seasonal abundance of phytoplankton groups in the South China Sea. *Progress in Oceanography*, *162*, 223–239. https://doi.org/10.1016/j.pocean.2018.03.008
Xie, Y., Laws, E. A., Yang, L., & Huang, B. (2018). Diel patterns of variable fluorescence and carbon fixation of picocyanobacteria prochlorococcus-dominated phytoplankton in the South China Sea Basin. *Frontiers in Microbiology*, *9*, 1589–1589. https://doi.org/10.3389/fmicb.2018.01589
Xu, M. N., Zhang, W., Zhu, Y., Liu, L., Zheng, Z., Wan, X. S., et al. (2018). Enhanced ammonia oxidation caused by Kuroshio intrusion in the boundary zone of the northern South China Sea. *Geophysical Research Letters*, *45*, 6585–6593. https://doi.org/10.1029/2018GL077896
Zhu, Y., Yuan, D., Huang, Y., Ma, J., & Feng, S. (2013). A sensitive flow-batch system for on board determination of ultra-trace ammonium in seawater: Method development and shipboard application. *Analytica Chimica Acta*, *794*(17), 47–54. https://doi.org/10.1016/j.aca.2013.08.009